



Facile synthesis of Yb_2O_3 –graphene nanocomposites for enhanced energy and environmental applications

T. Saravanan¹ · P. Anandan² · M. Shanmugam³ · M. Azhagurajan⁴ · M. Mohamed Ismail⁵ · M. Arivanandhan⁵ · Y. Hayakawa⁶ · R. Jayavel⁵

Received: 6 April 2019 / Revised: 12 June 2019 / Accepted: 7 September 2019 /

Published online: 10 September 2019

© Springer-Verlag GmbH Germany, part of Springer Nature 2019

Abstract

Graphene has been reduced from graphene oxide, and it has been used to prepare the Yb_2O_3 –graphene nanocomposites. Nanocomposites have been prepared by adding graphene with ytterbium oxide in 1, 3 and 5 weight percentage and named as $\text{Yb}_2\text{O}_3\text{G1}$, $\text{Yb}_2\text{O}_3\text{G3}$ and $\text{Yb}_2\text{O}_3\text{G5}$, respectively. Powder X-ray diffraction patterns have been obtained to study the structural identification. FTIR and laser Raman spectral analyses have been carried out to identify the functional groups and to confirm the formation of nanocomposites. The FESEM and HRTEM images have been obtained to study the morphology of the synthesized compounds. EPMA technique has been used to analyze the elemental composition by obtaining elemental mapping and energy-dispersive spectrum. The binding states of various elements present in the composites were analyzed and discussed using X-ray photoelectron spectra. The capacitance behavior and photocatalytic performance have been studied using electrochemical studies and optical absorption spectra. Significant enhancement of the capacitance behavior and the photocatalytic performance was observed as the presence of graphene increased in the composites.

Keywords Graphene · Nanocomposite · Rare earth · Cyclic voltammetry · Photocatalytic

Introduction

In the past few decades, rare earths and their oxide nanomaterials were intensively investigated and identified as potential materials for optoelectronics, photoluminescence and photocatalytic and in medical applications as well. Rare earth elements have played a vital role in the devices based on semiconductor compounds [1, 2]. Electroluminescent properties in III–V semiconductor compounds have been

✉ P. Anandan
anandantcet@gmail.com

Extended author information available on the last page of the article

studied by adding erbium as a dopant [3]. Blue, green and red fluorescence has been observed in fluoride glassed by doping europium [4]. Photoluminescence properties of europium nanowires doped with yttrium hydroxide and yttrium oxides have been studied and reported [5]. It has been reported that the increase in neodymium in tin oxide has enhanced the photoluminescence significantly [6]. The substitution of different rare earth elements for bismuth in bismuth–molybdenum oxide produced visible-light responsive compounds by gently red shifting the absorption edge to low-energy side [7].

On the other hand, carbon-based materials such as activated carbon, porous carbon and carbon nanotubes were broadly investigated for their suitability of this kind. The most advanced one-atom-thick planar sheet of sp^2 -bonded carbon atoms, graphene has created revolution in recent years in materials science and technology [8, 9]. Three-dimensional graphene-based materials have attracted great attention due to the specific surface area, low density, good electrical conductivity and excellent mechanical property [10]. Metal oxide- and graphene-based composite materials have recently attracted the attention, because of their extended storage, cyclic stability and photocatalytic properties [11, 12]. A wide range of nanostructured graphene-based materials have been investigated for flexible energy storage [13]. It has been reviewed that the functionalization of graphene materials by heteroatom doping has enhanced the energy conversion and storage as well [14] and covalently functionalized graphene has emerged as a very good electrode material [15]. However, it is understood that the rare earth oxide-based graphene composites were rarely investigated for their electrochemical properties. Hence, recently, our group has investigated the impact of graphene on the enhancement of electrochemical and photocatalytic performance of rare earth oxides [16–18].

In the present paper, Yb_2O_3 –graphene nanocomposites were prepared with different weight ratios of graphene with Yb_2O_3 . The composite materials were characterized by various analytical techniques. In addition to increased electrochemical performance, the photocatalytic performance was also observed as the composite increased having the higher percentage of graphene. Therefore, in this work, Yb_2O_3 G nanocomposite has been focused on energy storage and photocatalytic material.

Synthesis of graphene– Yb_2O_3 composite

To prepare the ytterbium oxide–graphene (Yb_2O_3 G) composites, 99 mg of as-purchased yttrium oxide (99.9%) was dispersed in 100 ml water by ultrasonication and 1 mg of synthesized graphene was added to the dispersion. Then, the solution was maintained at room temperature with constant stirring for 2 h. The final product Yb_2O_3 G1 was collected and dried in a vacuum at 60° C for 24 h. By the same procedure, Yb_2O_3 G3 and Yb_2O_3 G5 composites were also prepared by adding 97 mg Yb_2O_3 with 3 mg graphene and 95 mg Yb_2O_3 with 5 mg graphene, respectively. The influence of graphene on the structural, electrochemical and photocatalytic properties of ytterbium oxide has been studied by various techniques. The functional

properties such as cyclic voltammetric behavior and photocatalytic performance were analyzed by suitable methods.

Characterization techniques

The prepared nanocomposites were characterized by various analytical techniques. A Rigaku Mini FlexII-C X-ray diffractometer with $\text{CuK}\alpha$ ($\lambda = 1.540$ nm) radiation at a scanning rate of 1 deg/min was used to collect the powder X-ray diffraction data to identify the material. Raman and FTIR spectra were recorded to confirm the formation of composites JASCO Raman spectrophotometer (NRS-7100) and NICOLET infrared spectrophotometer, respectively. The morphology of the composites was analyzed using FESEM and HRTEM images obtained by JEOL 7001F and JEOL-JEM 2100F electron microscopes, respectively. The elemental composition was analyzed by elemental mapping and EDS spectra obtained by a JEOL JXA-8530F model field emission electron probe microanalyzer (FE-EPMA) instrument. The electron binding energies of various elements in the composites were analyzed by an ESCA 3400 SHIMADZU X-ray photoelectron spectrometer. The electrochemical performance of the composites was investigated by a three-electrode system using BioLogic electrochemical workstation. Glassy carbon, Ag/AgCl and platinum wire have been used as working, reference and counter electrodes, respectively. The cyclic voltammetric curves were recorded in the range from -0.1 to 0.4 at scan rates of 3, 10, 20, 30, 50, 60, 80 and 100 mV/s using 1 M H_2SO_4 as electrolyte. Photocatalytic performance of the nanocomposites was analyzed recording absorption changes in dye molecules using a CARY 500 Scan UV–Vis–NIR spectrophotometer.

Results and discussion

Powder X-ray diffraction studies

Powder X-ray diffraction patterns were recorded for the pure ytterbium oxide, $\text{Yb}_2\text{O}_3\text{G}$ nanocomposites and synthesized graphene as shown in Fig. 1a–e. The diffraction pattern of graphene contains only two peaks corresponding to 002 and 100 diffraction planes as shown in Fig. 1e. On the other hand, the diffraction patterns of ytterbium oxide and the composites have the large number of high-intense peak which ensures good crystalline nature as shown in Fig. 1a–d. The diffraction patterns have been compared with the standard JCPDS #65-3173 for cubic ytterbium oxide, and the peaks were indexed accordingly. From the powder diffraction patterns, it is inferred that the influence of graphene is not significant as the quantity of ytterbium oxide is high. On the careful examination of the enlarged peaks at various two-theta values, it was observed that the presence of graphene has shifted the peaks meagerly toward the lower diffraction angle and reduced the intensity of peaks (Fig. 2a, b). The observed peak shift is due to the lattice strain present in the $\text{Yb}_2\text{O}_3\text{G}$ composites.

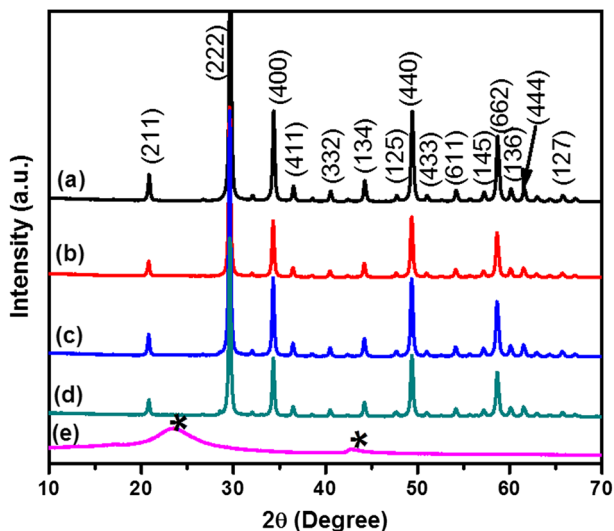


Fig. 1 Powder X-ray diffraction pattern of **a** pure Yb_2O_3 , **b** $\text{Yb}_2\text{O}_3\text{G1}$, **c** $\text{Yb}_2\text{O}_3\text{G3}$, **d** $\text{Yb}_2\text{O}_3\text{G5}$ composites and **e** synthesized graphene

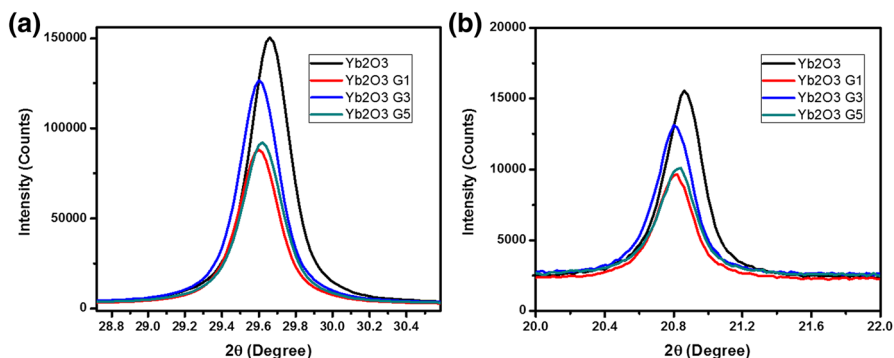


Fig. 2 Powder X-ray diffraction plane of **a** (222) and **b** (211) shows the mild peak shift toward lower angle

Laser Raman spectral studies

Laser Raman spectra have been recorded for the graphene, Yb_2O_3 , $\text{Yb}_2\text{O}_3\text{G1}$ and $\text{Yb}_2\text{O}_3\text{G5}$ composites between the wavenumber regions 100 and 2000 cm^{-1} . The spectrum of pure graphene does not have any peaks from 100 to 800 cm^{-1} (Fig. 3a), and the characteristic peaks are called D and G bands at 1343 and 1580 cm^{-1} , respectively, as shown in Fig. 3b. The intensity ratio of D and G band, I_D/I_G , for graphene has been measured as greater than 1 (1.11). Hence, the graphene reduced from GO is in ordered nature and has reasonably good quality and ensured the sp^2 -bonded carbon. On the other hand, the $\text{Yb}_2\text{O}_3\text{G1}$ and $\text{Yb}_2\text{O}_3\text{G5}$ composites are

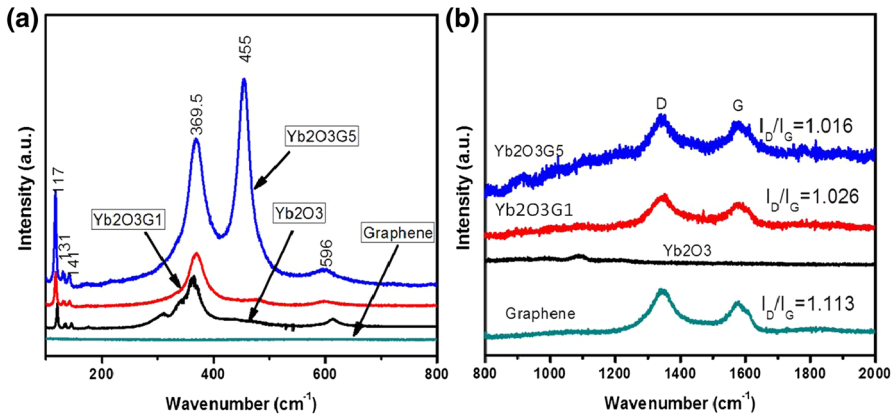


Fig. 3 Raman spectra of graphene and $\text{Yb}_2\text{O}_3\text{G}$ nanocomposites at region between **a** 100 and 800 cm^{-1} , **b** 800 and 2000 cm^{-1}

having more number of peaks in the region between 100 cm^{-1} and 800 cm^{-1} in addition to the D and G bands of graphene in the region of $800\text{--}2000\text{ cm}^{-1}$. These bands have not been shifted significantly; however, the intensity ratio between D and G bands has been reduced from 1.11 to 1.016 as the amount of graphene increased. The reduced intensity ratio and more number of peaks are the evidence for the formation of $\text{Yb}_2\text{O}_3\text{G5}$ composite. The additional peak at 455 cm^{-1} with higher intensity is due to the composite.

FTIR spectral studies

The presence of functional groups of $\text{Yb}_2\text{O}_3\text{G}$ composites has been identified by FTIR spectral analyses. The spectra have been recorded in the wavenumber range between $400\text{ and }4000\text{ cm}^{-1}$ as shown in Fig. 4. From the spectra, it has been observed that the band around 3500 cm^{-1} is due to the absorbed water from the atmosphere, which is much weaker in the composites compared to pure Yb_2O_3 . Generally, the stretching vibrations of CO_2 lie in the region between $3000\text{ and }1000\text{ cm}^{-1}$ which have appeared in the pure Yb_2O_3 FTIR spectrum due to the presence of atmospheric CO_2 . These bands were suppressed in the composites, and the absorption peak at 584 cm^{-1} is due to the stretching vibrations of Yb-O and this absorption weakened in $\text{Yb}_2\text{O}_3\text{G5}$ sample. The weak vibrations related to carbon and oxygen observed in the composites confirm the formation of $\text{Yb}_2\text{O}_3\text{G}$ composites.

Morphological analysis

Figures 5 and 6 are the FESEM images which show the morphology of pure Yb_2O_3 and composites, respectively. It can be observed from Fig. 5a that the pure Yb_2O_3 contains microcrystals with irregular shape. The magnified image shown in Fig. 5b ensured that Yb_2O_3 contains nano- and microcrystals. As shown in Fig. 6a, graphene

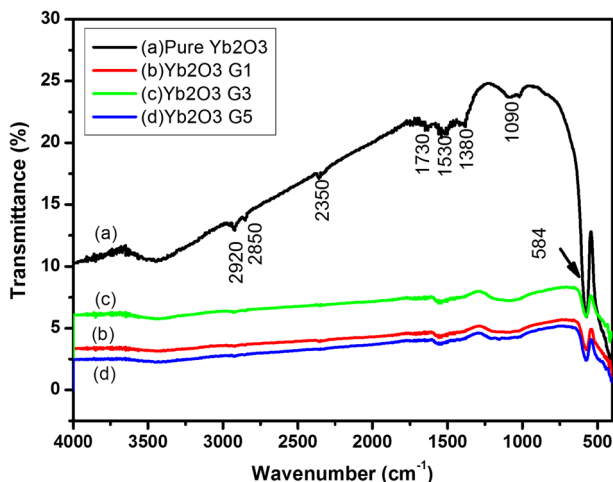


Fig. 4 FTIR spectra of **a** pure Yb_2O_3 , **b** $\text{Yb}_2\text{O}_3\text{G1}$, **c** $\text{Yb}_2\text{O}_3\text{G3}$ and **d** $\text{Yb}_2\text{O}_3\text{G5}$ nanocomposites

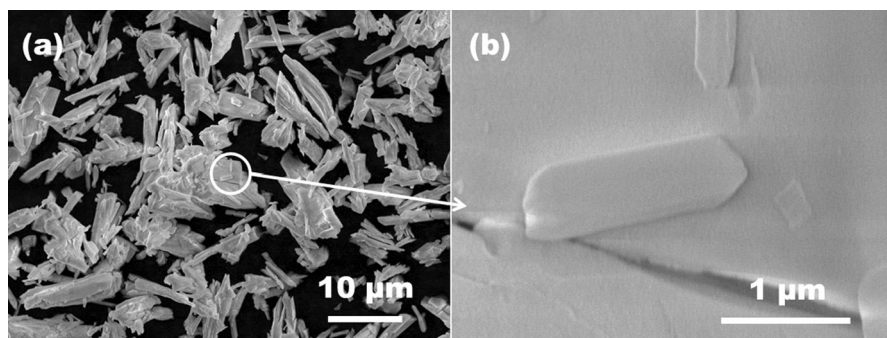


Fig. 5 FESEM images of pure Yb_2O_3 at different magnifications

sheets mixed in the midst of Yb_2O_3 crystals have been observed in the composite $\text{Yb}_2\text{O}_3\text{G1}$. The magnified image (Fig. 6b) ensured that the Yb_2O_3 crystals were covered by graphene and thereby the composites formed. The FESEM images of $\text{Yb}_2\text{O}_3\text{G5}$ composite (Fig. 6c, d) inferred that large amount of yttrium oxide crystals were involved in the formation of composite and the magnified image ensured the flake-like morphology of composite has been formed. The increase in graphene weight percent has caused the aggregation of Yb_2O_3 with graphene, and hence, graphene structure has become irregular flake-like structure as shown in Fig. 6d. Further, it is observed from the quality of the images that the graphene sheets have been effectively reduced from GO [16].

Figure 7a–d shows the HRTEM images of $\text{Yb}_2\text{O}_3\text{G5}$ at different magnifications. From the marked region of Fig. 7a, it is inferred that the Yb_2O_3 crystals are stacked in between graphene sheets. The magnified image infers that the size of the crystals is less than 100 nm as shown in Fig. 7b. The high-magnification images of marked region in

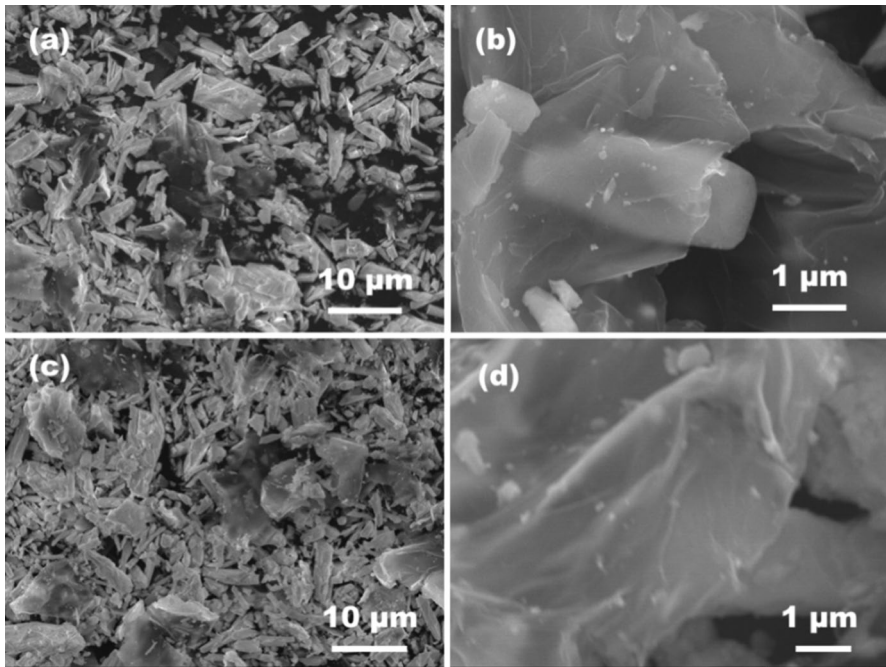


Fig. 6 FESEM images of **a, b** $\text{Yb}_2\text{O}_3\text{G1}$ and **c, d** $\text{Yb}_2\text{O}_3\text{G5}$ at different magnifications

Fig. 7b are shown in Fig. 7c, d. A few layers of graphene sheets as a portion of composite have been observed clearly (Fig. 7c). The Yb_2O_3 (Fig. 7d) crystal observed in the nanocomposite possesses the lattice fringes which are clearly seen in the image which ensured the crystalline nature, and the FFT pattern corresponding to Fig. 7d is shown in the inset.

Elemental analysis

Pure Yb_2O_3 , graphene and the prepared composites were subjected to electron probe microanalysis, and the elemental mapping was recorded. The FE-EPMA mapping ensures that the presence of ytterbium and carbon is significantly higher than that of oxygen as shown in Fig. 8. The corresponding energy-dispersive spectrum for $\text{Yb}_2\text{O}_3\text{G5}$ composite is shown in Fig. 9. The elemental composition of carbon, oxygen and ytterbium elements was estimated for Yb_2O_3 , $\text{Yb}_2\text{O}_3\text{G1}$ and $\text{Yb}_2\text{O}_3\text{G5}$ composites and is listed in Table 1. It is observed that the atomic percentage of ytterbium in the selected region of the composite has been decreased well as the carbon level increased.

X-ray photoelectron spectral analysis

The survey spectrum of $\text{Yb}_2\text{O}_3\text{G5}$ composite has been recorded by an X-ray photoelectron spectrometer as shown in Fig. 10a. It has sound signals for oxygen and

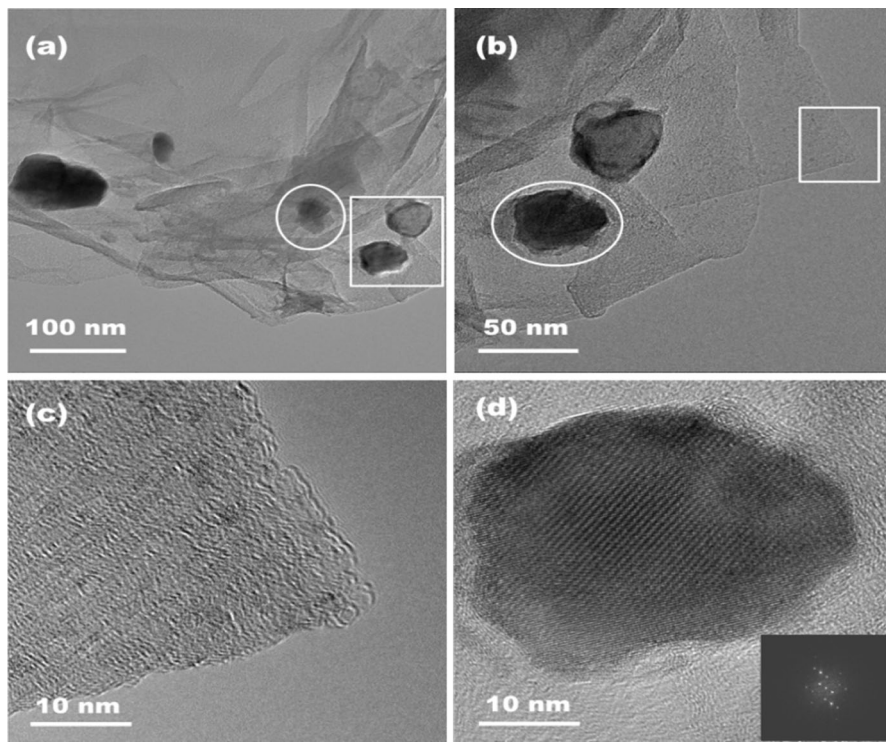


Fig. 7 HRTEM images of $\text{Yb}_2\text{O}_3/\text{G5}$ nanocomposite from lower to higher magnification

carbon 1s electron; but the signal for ytterbium 4d electron could not be identified in the survey spectrum. Hence, the core-level XPS spectra of various elements for $\text{Yb}_2\text{O}_3/\text{G5}$ composite have been obtained. The core-level spectrum of 4d of ytterbium in the region of 170–210 eV with a peak at 186.3 eV is shown in Fig. 10b. The core-level XPS spectrum of C 1s is shown in Fig. 10c, which contains two peaks at 285.1 and 288.9 eV due to sp^2 -bonded carbon (C–C) and carboxyls (C–O), respectively. This indicates carbon has a reasonable amount of oxygen containing functional groups capable of enhancing the photocatalysis by trapping the photoinduced holes [12], which increases the formation of highly oxidizing OH radicals [19]. Two different oxygen species could be distinguished clearly by observing O1s spectrum in the range between 525 and 540 eV as shown in Fig. 10d. The binding energies of 530.8 and 532.6 eV have been assigned to lattice oxygen and hydroxyl groups, respectively [12].

Cyclic voltammetric behavior

Cyclic voltammetric measurements of $\text{Yb}_2\text{O}_3/\text{G}$ nanocomposites were taken in an aqueous solution of 1 M H_2SO_4 with the potential range of -0.1 to 0.4 V. The redox behavior of metal oxides and composites was observed for different

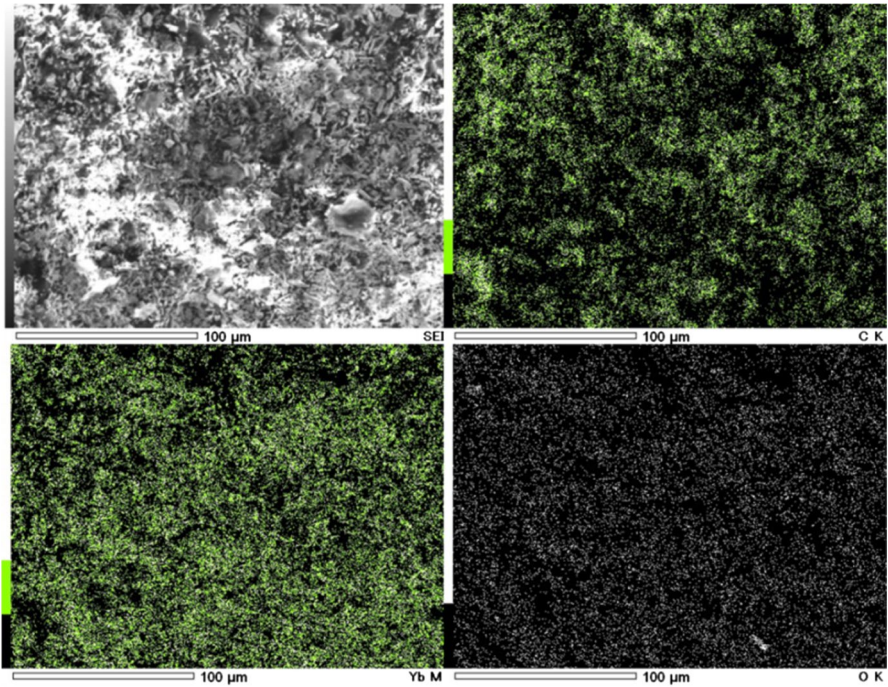


Fig. 8 FE-EPMA images of $\text{Yb}_2\text{O}_3\text{G5}$

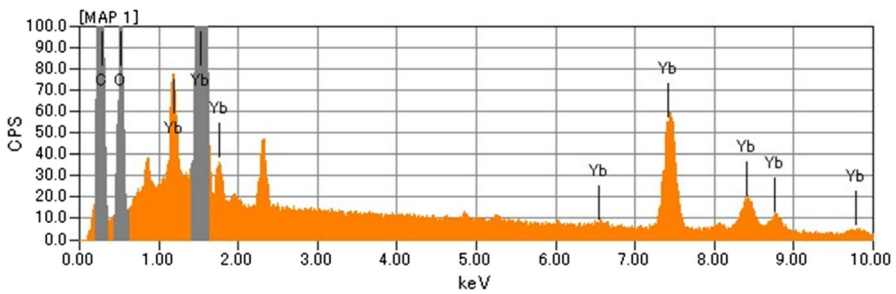
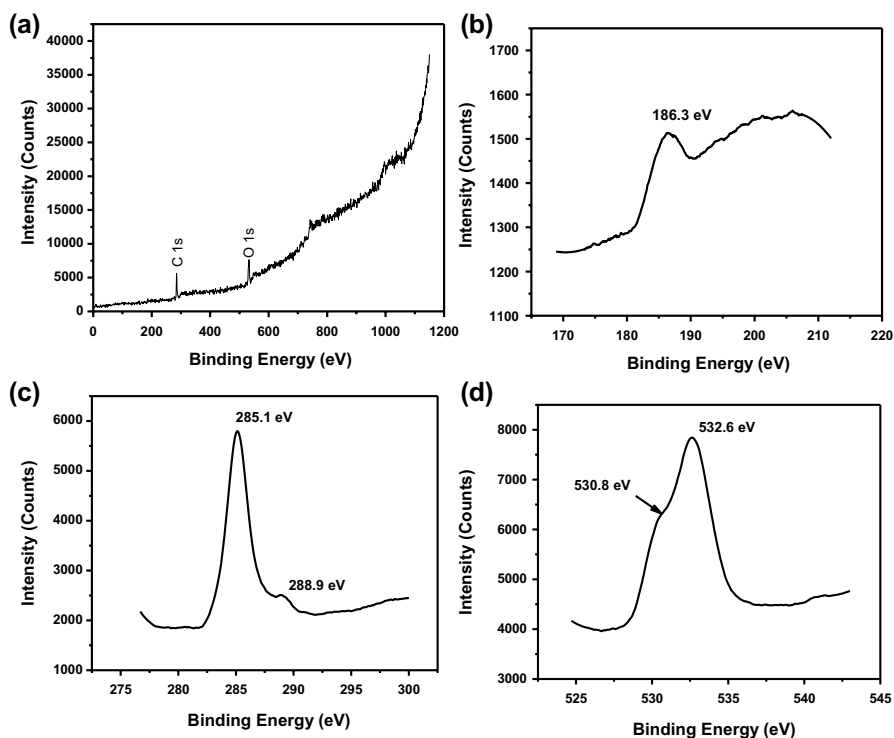


Fig. 9 Energy-dispersive spectrum of $\text{Yb}_2\text{O}_3\text{G5}$

scanning rates from 3 to 100 mV/s. The recorded voltammogram of pure Yb_2O_3 , $\text{Yb}_2\text{O}_3\text{G1}$ and $\text{Yb}_2\text{O}_3\text{G5}$ for different scanning rates is shown in Fig. 11a–c. Nearly rectangular smooth CV loops were observed with a mild redox behavior, which ensures the pseudocapacitance behavior of the materials. It is found that the current and integral area of the CV loop have increased when the scan rate was increased, which indicates the good capacitance behavior of nanocomposites. The CV measurements for pure Yb_2O_3 and $\text{Yb}_2\text{O}_3\text{G}$ composites for the lowest scanning rate (3 mV/s) in the present study have been compared and the

Table 1 Measured elemental composition of reduced graphene and $\text{Yb}_2\text{O}_3\text{G}$ composites

Sample	Element	Atomic %	Error
Graphene	C K	85.67	0.12
	O K	14.33	1.23
Yb_2O_3	Yb L	36.97	0.79
	O K	63.03	0.29
$\text{Yb}_2\text{O}_3\text{G1}$	Yb L	7.92	0.58
	C K	69.79	0.09
$\text{Yb}_2\text{O}_3\text{G5}$	O K	22.30	0.28
	Yb L	4.90	0.56
	O K	75.88	0.08
	O K	19.22	0.30

**Fig. 10** **a** X-ray photoelectron survey spectrum of $\text{Yb}_2\text{O}_3\text{G5}$, core-level X-ray photoelectron spectra of **b** ytterbium $4d$ electron, **c** carbon $1s$ electron and **d** oxygen $1s$ electron in the $\text{Yb}_2\text{O}_3\text{G5}$ composite

voltammograms are shown in Fig. 11d. It is found that the current density has increased as the graphene content in the composite increased. From the results, it is obvious that the increase in the current density as influenced by graphene reveals the amount of graphene added in the present investigation has enhanced

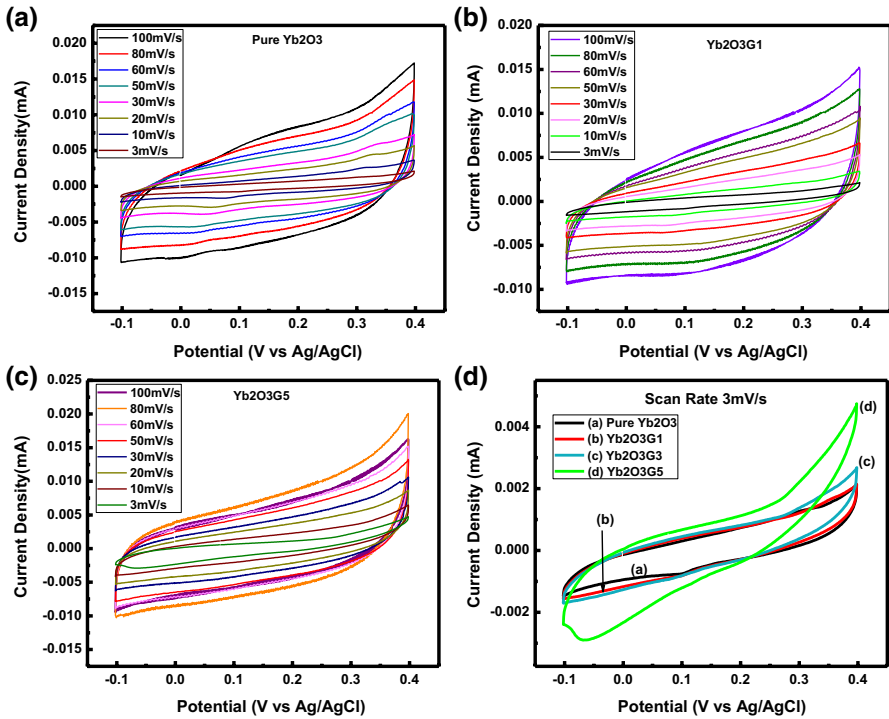


Fig. 11 Cyclic voltammograms for **a** pure Yb₂O₃, **b** Yb₂O₃G1, **c** Yb₂O₃G5 nanocomposites at different scan rates and **d** comparison of CV loop of pure Yb₂O₃, Yb₂O₃G1, Yb₂O₃G3 and Yb₂O₃G5 for the scanning rate of 3 mV/s

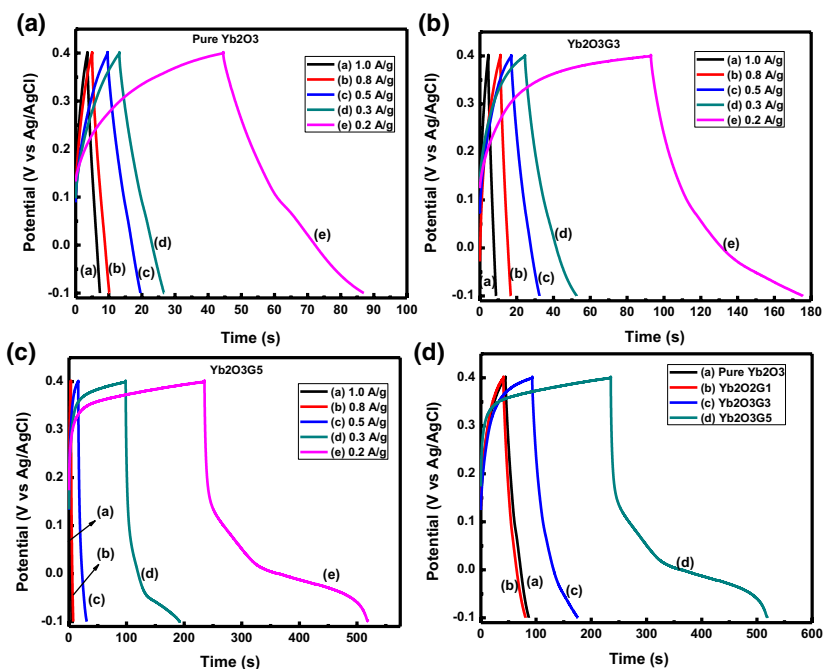
the double-layer capacitance behavior [18]. The specific capacitance values of Pure Yb₂O₃ and Yb₂O₃G composites for different scanning rates also have been calculated under the area of CV curves using the equation [16]

$$C_s = \int IdV/vmV \tag{1}$$

where *I* is the response current, *V* is the potential, *v* is the potential scan rate and *m* is the mass of the active material on the electrode. The calculated specific capacitance values are listed in Table 2. For all the materials, the specific capacitance value has decreased as the scan rate increased. Maximum specific capacitance value of 550 F/g for Yb₂O₃G5 sample has been observed at a scan rate of 3 mV/s. The decrease in specific capacitance values in response to the increase in scan rate indicates that the electrochemical capacitive process has been controlled by concentration polarization or diffusion electrochemistry [18]. On the other hand, the charge–discharge curves of pure Yb₂O₃, Yb₂O₃G1, Yb₂O₃G3 and Yb₂O₃G5 have also been recorded for different current densities and are shown in Fig. 12a–c. It has been observed that the discharge time has been increased as the current density has been decreased. The discharge time has also been noted from the comparison as

Table 2 Calculated specific capacitance values of pure Yb_2O_3 , $\text{Yb}_2\text{O}_3\text{G1}$, $\text{Yb}_2\text{O}_3\text{G3}$ and $\text{Yb}_2\text{O}_3\text{G5}$ composites for different scan rates

Scan rate (mV/s)	Specific capacitance of pure Yb_2O_3 (F/g)	Specific capacitance of $\text{Yb}_2\text{O}_3\text{G1}$ (F/g)	Specific capacitance of $\text{Yb}_2\text{O}_3\text{G3}$ (F/g)	Specific capacitance of $\text{Yb}_2\text{O}_3\text{G5}$ (F/g)
3	303	326	352.24	550
10	202	199	222	273.2
20	195	191	206	268
30	178	173	189.33	232.6
50	157.2	151.6	163.2	184.4
60	150	144	155.33	174.33
80	138	131.7	139.25	131
100	129.8	122.6	128.2	129.2

**Fig. 12** Galvanostatic charge–discharge curves for **a** pure Yb_2O_3 , **b** $\text{Yb}_2\text{O}_3\text{G3}$, **c** $\text{Yb}_2\text{O}_3\text{G5}$ nanocomposites at different current densities and **d** comparison of CD curves of pure Yb_2O_3 , $\text{Yb}_2\text{O}_3\text{G1}$, $\text{Yb}_2\text{O}_3\text{G3}$ and $\text{Yb}_2\text{O}_3\text{G5}$ for the current density of 0.2 A/g

shown in Fig. 12d as significantly increased due to the increase in graphene content in the composite.

Photocatalytic property

The photocatalytic activity of the prepared composites for dye degradation was tested on MB dye under UV irradiation, and the results are shown in Fig. 13. The dye degradation experiment was performed for pure Yb_2O_3 and $\text{Yb}_2\text{O}_3\text{G}$ composites at the same period of UV light irradiation. The aqueous solutions of MB dye with pure Yb_2O_3 and $\text{Yb}_2\text{O}_3\text{G}$ nanocomposites were irradiated by UV light for 30 min, and the variation of the characteristic absorption peaks of MB dye at 662 nm and a shoulder peak at 610 nm was observed. As shown in the figure, the percentage of graphene in the composite influenced significantly on the dye degradation activity and found that $\text{Yb}_2\text{O}_3\text{G5}$ has better catalytic activity than that of other $\text{Yb}_2\text{O}_3\text{G}$ composites and pure Yb_2O_3 . It is observed that 40% of dye has been degraded in 30-min duration of UV radiation in the dye solution containing $\text{Yb}_2\text{O}_3\text{G5}$ composite. However, the same has been observed as 25, 17 and 3% for the dye solutions containing $\text{Yb}_2\text{O}_3\text{G3}$, $\text{Yb}_2\text{O}_3\text{G1}$ and Yb_2O_3 composites, respectively.

The photodegradation process is mainly depending on the generation of photoinduced charge carriers (electron–hole pair), charge separation and its migration to the surface. In the surfaces, surface hydroxyl traps the electrons and holes to form the hydroxyl radicals [18]. Yb_2O_3 is a good photocatalytic material due to its high valance band (VB) potential, which results in the formation of holes with high oxidative ability and thus can oxidize OH^- into OH radicals. On the other hand, the dye adsorption would be higher in the nanocomposites than that in the pure Yb_2O_3 due to high surface area of graphene [18]. Moreover, the oxygen content is low in the prepared reduced graphene as confirmed in EPMA analysis (Table 1) and thus the oxygen reaction sites like C–O groups are limited in the nanocomposite with low graphene content ($\text{Yb}_2\text{O}_3\text{G1}$ and $\text{Yb}_2\text{O}_3\text{G3}$). The high dye adsorption and the

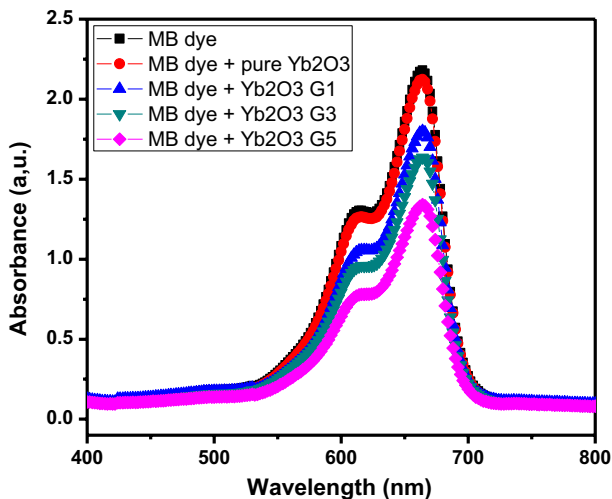


Fig. 13 Absorption spectra of MB dye, MB dye with Yb_2O_3 and MB dye with $\text{Yb}_2\text{O}_3\text{G}$ nanocomposites after the solution is irradiated by UV light for 30 min

low oxygen content cause low photocatalytic activity in the samples $\text{Yb}_2\text{O}_3\text{G1}$ and $\text{Yb}_2\text{O}_3\text{G3}$. At the higher mole percent of graphene ($\text{Yb}_2\text{O}_3\text{G5}$), the oxygen reaction sites are increased due to the large amount of graphene in the composite. Moreover, the oxide and hydroxyl radicals were increased in the samples, which resulted in better photocatalytic performance. In addition, the Yb_2O_3 -graphene nanocomposite retards the recombination of excitons, which leads to efficient charge separation. As discussed in the XPS analysis, the presence of hydroxyl group and surface oxygen in the nanocomposite increases the OH and oxygen radical formations. Formation of such radicals is responsible for the decomposition of dye molecules [20, 21].

Conclusion

Graphene reduced from graphene oxide was used to prepare the Yb_2O_3 -graphene nanocomposites. Nanocomposites were prepared by adding graphene with ytterbium oxide in different weight percentages. Structural studies were carried out by powder X-ray diffraction method. FTIR and laser Raman spectral analyses were carried out to identify the functional groups and to confirm the formation of nanocomposites. The morphology of the synthesized compounds has been studied by FESEM and HRTEM images. Elemental mapping and energy-dispersive spectrum were analyzed by EPMA technique. X-ray photoelectron spectra were analyzed, and the binding states of various elements present in the composites were discussed. The electrochemical studies show that the Yb_2O_3 -graphene nanocomposites exhibit good capacitance behavior, and large specific capacitance value of 550 F/g for $\text{Yb}_2\text{O}_3\text{G5}$ composite at the scanning rate of 3 mV/s has been observed. The discharge time has increased seven times greater for $\text{Yb}_2\text{O}_3\text{G5}$ composite when compared to pure Yb_2O_3 . In addition, the photocatalytic performance has been observed to be significantly increased as the presence of graphene increased in the composites.

Compliance with ethical standards

Conflict of interest The authors declare that they have no conflict of interest.


References

1. Zakharenkov LF (1995) Rare-earths: application in bulk III–V semiconductor crystal growth technology. *Microelectron J* 26(1):55–67
2. Gorelenok AT, Kamanin AV, Shmidt NM (1995) Rare-earth elements in the technology of InP, nGaAsP and devices based on these semiconductor compounds. *Microelectron J* 26(7):705–723
3. Zavada JM, Zhang D (1995) Luminescence properties of erbium in III–V compound semiconductors. *Solid-State Electronics* 38(7):1285–1290
4. Dejneka M, Snitzer E, Riman RE (1995) Blue, green and red fluorescence and energy transfer of Eu^{3+} in fluoride glasses. *J Lumin* 65(5):227–245
5. Xingcai Wu, Tao Yourong, Gao Fei, Dong Lin, Zheng Hu (2005) Preparation and photoluminescence of yttrium hydroxide and yttrium oxide doped with europium nanowires. *J Cryst Growth* 277(1–4):643–649

- Hild F, Eichenberger L, Bouché A, Devaux X, Stoffel M, Rinnert H, Vergnat M (2015) Structural and photoluminescence properties of evaporated SnO₂ thin films doped with rare earths. *Energy Procedia* 84:141–148
- Sandhya Kumari L, Prabhakar Rao P, Sameera S, James Vineetha, Koshy Peter (2015) Effects of rare earth substitution on the optical properties of Bi₂MoO₆ for coloring applications. *Mater Res Bull* 70:93–98
- Geim AK, Novoselov KS (2007) The rise of graphene. *Nat Mater* 6:183–191
- Dikin DA, Stankovich S, Zimney EJ, Piner RD, Dommett GHB, Evmenenko G, Nguyen ST, Ruoff RS (2007) Preparation and characterization of grapheme oxide. *Nature* 448:457–460
- Fan Xueliu, Chen Xuli, Dai Liming (2015) 3D graphene based materials for energy storage. *Curr Opin Colloid Interface Sci* 20(5–6):429–438
- Perera SD, Mariano RG, Vu K (2012) Hydrothermal synthesis of graphene–TiO₂ nanotube composites with enhanced photocatalytic activity. *ACS Catalysis* 2:949–956
- Chen Y, Song BH, Tang HS, Lu L, Xue JM (2012) One step synthesis of hallow porous Fe₃O₄ beads-reduced graphene oxide composites with superior battery performance. *J Mater Chem* 22:17656–17662
- Guo Xiaotian, Zheng Shasha, Zhang Guangxun, Xiao Xiao, Li Xinran, Yuxia Xu, Xue Huaiguo, Pang Huan (2017) Nanostructured graphene-based materials for flexible energy storage. *Energy Storage Materials* 9:150–169
- Chuangang Hu, Liu Dong, Xiao Ying, Dai Liming (2018) Functionalization of graphene materials by heteroatom-doping for energy conversion and storage. *Progress in Natural Science: Materials International* 28(2):121–132
- Bakandritsos Aristides, Jakubec Petr, Pykal Martin, Otyepka Michal (2018) Covalently functionalized graphene as a supercapacitor electrode material. *FlatChem* 13:25–33
- Saravanan T, Shanmugam M, Anandan P, Azhagurajan M, Pazhanivel K, Arivanandhan M, Hayakawa Y, Jayavel R (2015) Facile synthesis of graphene–CeO₂ nano nanocomposite with enhanced electrochemical properties for supercapacitors. *Dalton Trans* 44:9901
- Saravanan T, Anandan P, Shanmugam M, Azhagurajan M, Pazhanivel K, Arivanandhan M, Hayakawa Y, Jayavel R (2016) Synthesis and characterization of Y₂O₃-reduced graphene oxide nanocomposites for photocatalytic applications. *Mater. Res. Express* 3:075502
- Saravanan T, Anandan P, Shanmugam M, Jayakumari T, Arivanandhan M, Azhagurajan M, Hayakawa Y, Jayavel R (2018) Impact of graphene on the enhancement of electrochemical and photocatalytic performance of Gd₂O₃-graphene nanocomposites. *Solid State Sci* 83:171–180
- Xu J, Chang Y, Zhang Y, Ma S, Qu Y, Xu C (2008) Effect of silver ions on the structure of ZnO and photocatalytic performance of Ag/ZnO composites. *Applied Surface Sciences* 255:1996–1999
- Li YF, Xu D, Oh JI, Shen W, Li X, Yu Y (2012) Mechanistic study of co-doped titania with non-metal and metal ions: a case of C + Mo codoped TiO₂. *ACS Catalysis* 2:391–398
- Wu YF, Zhang QJ, Yin XF, Cheng HQ (2013) Template-free synthesis of mesoporous anatase yttrium-doped TiO₂ nanosheet-array films from waste bicolor fluorescent powder with high photocatalytic activity. *RSC Adv* 3:9670–9676

Publisher's Note Springer Nature remains neutral with regard to jurisdictional claims in published maps and institutional affiliations.

Affiliations

T. Saravanan¹ · P. Anandan²  · M. Shanmugam³ · M. Azhagurajan⁴ · M. Mohamed Ismail⁵ · M. Arivanandhan⁵ · Y. Hayakawa⁶ · R. Jayavel⁵

¹ Centre for Materials Research, Thiruvalluvar College of Engineering and Technology, Vandavasi 604 505, India

² Department of Physics, Thiru Kolanjiappar Government Arts College, Vriddhachalam 606 001, India

- ³ Department of Civil Engineering, Disasters Prevention Research Institute, Yeungnam University, Gyeongsan 38541, Republic of Korea
- ⁴ Frontier Research Institute for Interdisciplinary Sciences, Tohoku University, Sendai 980 858, Japan
- ⁵ Centre for Nanoscience and Technology, Anna University, Chennai 600 025, India
- ⁶ Research Institute of Electronics, Shizuoka University, Johoku, Naka-ku, Hamamatsu 432 8011, Japan